Nonlinear Deformation of a Thermally Stressed Graphite Annular Disk

Robert M. Jones*
Southern Methodist University, Dallas, Texas
and
H. Stuart Starrett†
Southern Research Institute, Birmingham, Ala.

An ATJ-S graphite annular disk of a wedge-shaped cross section is subjected to outside to inside temperature gradients of up to 3000°F from an induction heating coil. The change in internal diameter of the disk is measured with a laser tracking device and is predicted with a modification of the Jones-Nelson nonlinear material model. This model is shown to be valid for ATJ-S graphite, which is a transversely isotropic granular composite material with stress-strain behavior that is highly nonlinear, strongly dependent on temperature, and different in tension than in compression. The predicted diameter changes at three times in the same test agree with the averages of two perpendicular diameter change measurements within about 3%.

Nomenclature

A_i, B_i, C_i, U_{0_i}	= constants in ith mechanical property equation [Eq. (1)]
E_r, E_z, E_θ	= Young's moduli in principal material directions
E_{rz}^{45}	= Young's modulus at 45° to r and z directions
r, z, θ	= radial, axial, and circumferential directions (Fig. 1)
t	= time, sec
T	= temperature, °F
U	= strain energy density [Eq. (2)]
$\epsilon_r, \epsilon_z, \epsilon_\theta, \gamma_{rz}$	= axisymmetric strains in principal material directions
$\nu_{rz}, \nu_{r\theta}, \nu_{z\theta}$	= Poisson's ratios for principal material directions
$\sigma_r, \sigma_z, \sigma_\theta, \tau_{rz}$	= axisymmetric stresses in principal material directions
Subscripts	
c	= compression
t	= tension

Introduction

ATJ-S graphite is a transversely isotropic granular or particulate composite material made in cylindrical billet form, as shown in Fig. 1 along with the coordinates used in this paper. The flake-like graphite particles are aligned in planes of isotropy during billet compaction in the z direction. The resulting material stress-strain behavior is highly nonlinear and strongly temperature-dependent, as displayed for the r-θ plane in Fig. 2. There, the boxes are actual experimental data reported by Starrett and Pears,[1] and the curves are the Jones-Nelson nonlinear material model[2-6] fits to the data. In Fig. 2, the tension behavior becomes stiffer as the temperature approaches 2000°F, and even stiffer at 3000°F. However, the stress-strain curve at 3000°F is slightly lower for high strains than that at 2000°F. The compression behavior for the r-θ plane monotonically becomes more flexible as the temperature increases from 3000° to 5000°F. Moreover, the stress-strain behavior is different under tension loading than under compression loading at every temperature, although the two behaviors are shown here only for 3000°F.

The objective of this paper is to extend the qualification of the Jones-Nelson nonlinear material model[2-6] from mechanical loading problems for homogeneous bodies to thermal loading problems for nonhomogeneous bodies. The previous level of qualification of the model is to uniaxial off-axis mechanical loading problems[3,6] and to biaxial mechanical loading problems in principal material directions for ATJ-S graphite.[2,6] The multimodulus character (moduli or stiffnesses that are different in tension than in compression) is treated by Jones and Nelson,[5,6] but nonhomogeneous bodies due to temperature-dependent behavior have not been addressed with this model. Part of the motivation for this extension of the model is the use of ATJ-S graphite in re-entry vehicle nosetips, where substantial temperature gradients exist. These temperature gradients lead to thermal stresses for which the associated nonlinear deformations must be predicted in order to design nosetips and other structural elements rationally and accurately.

The simplest vehicle to accomplish the objective of qualifying the model for thermal loading problems is the Southern Research Institute (SoRI) thermal stress disk test.[7] In this test, an annular disk is heated rapidly at its outer diameter, resulting in an outside to inside diameter temperature gradient. The outside portion of the disk tends to expand more than the inside so thermal stresses are generated. In the circumferential direction, the stresses are compressive near the outer diameter and tensile near the inner diameter. The level of both the compressive and tensile stresses is important because the original purpose of the SoRI thermal

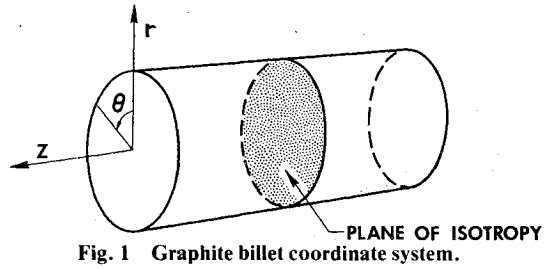

Fig. 1 Graphite billet coordinate system.

Presented as Paper 77-425 at the AIAA/ASME 18th Structures, Structural Dynamics, and Materials Conference, San Diego, Calif., March 21-23, 1977; (in bound volume of Conference papers): received Jan. 24, 1977; revision received April 25, 1977.

Index categories: Structural Composite Materials; Materials, Properties of; Thermal Stresses.

*Professor of Solid Mechanics. Associate Fellow AIAA.

†Head, Analytical Section, Mechanical Engineering Division.

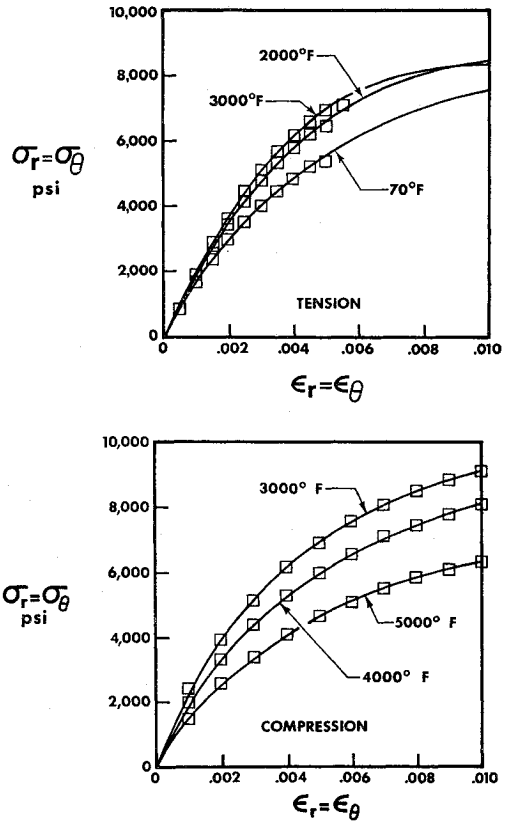

Fig. 2 Temperature-dependent nonlinear multimodulus stress-strain behavior of ATJ-S graphite.

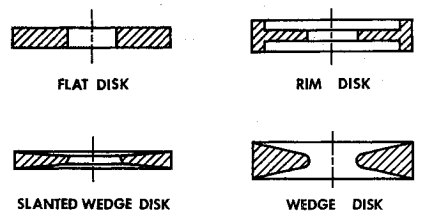

Fig. 3 Annular disk cross sections.

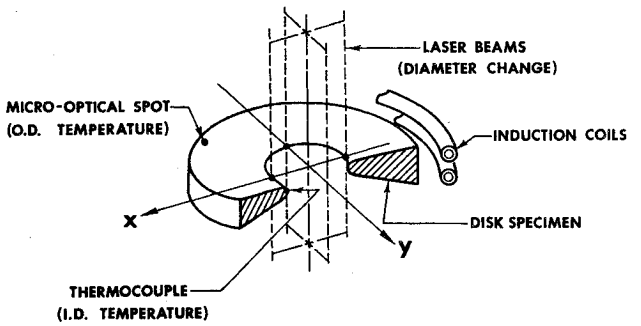

Fig. 4 Schematic of SoRI thermal stress disk test.

stress disk test was to fail disks of many different graphites quickly and easily so that their relative merits could be assessed. The failures almost invariably occur in the region of tensile stress. Accordingly, the compressive stresses must be high enough to generate (self-equilibrating) tensile stresses that will cause failure. The tensile stresses are too low for the simple flat annular disk and the rim disk in Fig. 3. That is, not enough disk material is in compression to force high enough tensile stresses for fracture to occur in some of the better aerospace-grade graphites (although some lower-grade graphites can be fractured). However, the disks with a wedge-shaped cross section in Fig. 3 do have high enough tensile stresses to cause fracture in ATJ-S graphite. The slanted wedge disk has an inclined inner diameter surface to provide a well-defined target for the laser diameter measuring device, which will be discussed later. The inner diameter of the wedge disk in Fig. 3 is, however, sufficiently well-defined to provide a good target. Thus, the simple wedge disk is used in the theoretical-experimental correlation studies.

This paper is divided in two major sections: 1) measurement of temperatures and deformations and 2) prediction of deformations, stresses, and strains. In the measurements section, the overall test setup is described, along with the character of the individual measurements that are made. In the predictions section, the Jones-Nelson nonlinear material model and its extensions for the present problem are described, along with the modeling of ATJ-S graphite. Moreover, the predicted diameter changes are compared with the measured values. Finally, the stress and strain state in the disk is displayed and discussed.

Measurement of Temperatures and Deformations

Overall Test Setup

The SoRI thermal stress disk test[7] is essentially a tension test. The stresses are induced solely through rapid thermal deformation, which is constrained because of the disk geometry. Radial temperature gradients are generated in the disk with induction heating, as shown in Fig. 4. The power from the induction heating coils is initially concentrated in the outer periphery of the disk (about 85% in the outer 0.10 in.), while the inside remains relatively cool. Many factors enter in the proper matching of the power supply to the test specimen, but the major considerations include coil design, specimen material, specimen design, and specimen-to-coil proximity. The disk is made with its diameter in the graphite plane of isotropy shown in Fig. 1. The disk is not fastened to the test fixture, but is positioned horizontally as in Fig. 4, and rests on a smooth surface.

Several measurements are made during a single test run for an individual specimen: 1) a temperature measurement at the inner diameter, 2) a temperature measurement at a point near the outer diameter, and 3) measurements of the diametral deformations along two orthogonal axes of the internal hole. Each of these measurements is discussed in the following subsections.

Inner Diameter Temperature Measurement

The temperature at the disk inner diameter is measured with a thermocouple probe. The fine thermocouple wires (10×10^{-3} in.) are not welded together, but instead are spring pressed on the disk so that the graphite makes the junction. This procedure is used to avoid a weld bead, which invariably leads to distortion of the parent material thermal characteristics and to errors of several hundred degrees at the heating rates used in this test.

The thermocouple probe is calibrated by obtaining a steady-state reading between 1200° and 2000°F for a graphite specimen, and comparing that reading with the reading from an optical pyrometer, which is corrected for emittance. The error due to the graphite junction is on the order of 70° at 1500°F. Then, typical rapid heating runs are made, and the thermocouple probe reading is compared to a micro-optical reading, which is calibrated to a hand-held optical pyrometer. Thus, the basic calibration is for a range from the upper bound at the steady-state reference to the lower bound at the calibration to the hand optical pyrometer through the micro-optical recorder. The temperature at the inside diameter is known to within 5°F in any run.

Outer Diameter Temperature Measurement

The temperature at the disk outer diameter is measured with a micro-optical recorder as a function of time. Thus, the temperature reading is subject to the errors normally

Table 1 Jones-Nelson nonlinear material model parameters for ATJ-S(WS) graphite as a function of temperature

Temperature	Mechanical property	A	B	C
70°F	E_{r_t}	2.00×10^6 psi	0.182	0.337
	E_{z_t}	1.50×10^6 psi	0.226	0.322
	$\nu_{r\theta_t}$	0.110	0.0	1.0
	$\nu_{z\theta_t}$	0.090	0.0	1.0
	$E^{45}_{rz_t}$	1.55×10^6 psi	0.200	0.330
	E_{r_c}	3.00×10^6 psi	0.477	0.125
	E_{z_c}	2.10×10^6 psi	0.451	0.134
	$\nu_{r\theta_c}$	0.065	0.0	1.0
	$\nu_{z\theta_c}$	0.065	0.0	1.0
	$E^{45}_{rz_c}$	2.40×10^6 psi	0.470	0.130
2000°F	E_{r_t}	2.00×10^6 psi	0.0651	0.583
	E_{z_t}	1.60×10^6 psi	0.165	0.336
	$\nu_{r\theta_t}$	0.130	0.0	1.0
	$\nu_{z\theta_t}$	0.107	0.0	1.0
	$E^{45}_{rz_t}$	1.83×10^6 psi	0.120	0.460
	E_{r_c}	3.00×10^6 psi	0.333	0.203
	E_{z_c}	1.90×10^6 psi	0.281	0.221
	$\nu_{r\theta_c}$	0.082	0.0	1.0
	$\nu_{z\theta_c}$	0.082	0.0	1.0
	$E^{45}_{rz_c}$	2.84×10^6 psi	0.350	0.210
3000°F	E_{r_t}	2.10×10^6 psi	0.0510	0.660
	E_{z_t}	1.45×10^6 psi	0.0254	0.921
	$\nu_{r\theta_t}$	0.140	0.0	1.0
	$\nu_{z\theta_t}$	0.116	0.0	1.0
	$E^{45}_{rz_t}$	2.11×10^6 psi	0.0380	0.790
	E_{r_c}	3.60×10^6 psi	0.350	0.198
	E_{z_c}	1.80×10^6 psi	0.194	0.291
	$\nu_{r\theta_c}$	0.090	0.0	1.0
	$\nu_{z\theta_c}$	0.090	0.0	1.0
	$E^{45}_{rz_c}$	3.27×10^6 psi	0.310	0.240
3500°F	E_{r_t}	2.40×10^6 psi	0.277	0.212
	E_{z_t}	1.40×10^6 psi	0.133	0.395
	$\nu_{r\theta_t}$	0.145	0.0	1.0
	$\nu_{z\theta_t}$	0.120	0.0	1.0
	$E^{45}_{rz_t}$	2.04×10^6 psi	0.158	0.388
	E_{r_c}	3.60×10^6 psi	0.316	0.220
	E_{z_c}	2.00×10^6 psi	0.158	0.347
	$\nu_{r\theta_c}$	0.0950	0.0	1.0
	$\nu_{z\theta_c}$	0.0950	0.0	1.0
	$E^{45}_{rz_c}$	3.27×10^6 psi	0.270	0.290
4000°F	E_{r_t}	2.70×10^6 psi	0.282	0.237
	E_{z_t}	1.40×10^6 psi	0.107	0.477
	$\nu_{r\theta_t}$	0.150	0.0	1.0
	$\nu_{z\theta_t}$	0.125	0.0	1.0
	$E^{45}_{rz_t}$	1.97×10^6 psi	0.200	0.360
	E_{r_c}	2.80×10^6 psi	0.323	0.212
	E_{z_c}	1.80×10^6 psi	0.153	0.377
	$\nu_{r\theta_c}$	0.100	0.0	1.0
	$\nu_{z\theta_c}$	0.100	0.0	1.0
	$E^{45}_{rz_c}$	3.06×10^6 psi	0.270	0.300
4500°F	E_{r_t}	2.50×10^6 psi	0.300	0.250
	E_{z_t}	1.30×10^6 psi	0.100	0.500
	$\nu_{r\theta_t}$	0.170	0.0	1.0
	$\nu_{z\theta_t}$	0.150	0.0	1.0
	$E^{45}_{rz_t}$	1.50×10^6 psi	0.200	0.400
	E_{r_c}	2.40×10^6 psi	0.275	0.250
	E_{z_c}	1.80×10^6 psi	0.244	0.267
	$\nu_{r\theta_c}$	0.150	0.0	1.0
	$\nu_{z\theta_c}$	0.150	0.0	1.0
	$E^{45}_{rz_c}$	2.40×10^6 psi	0.300	0.270

associated with optically measuring the temperature of a gray body plus the errors peculiar to the particular specimen and to this system. The latter errors include those peculiar to transient measurements, plus those resulting from the existence of a 200°F temperature gradient over the field of view of the recorder. That is, the recorder is focused on a spot as in Fig. 4 on the *top* surface of the disk, since the outer diameter surface is covered by the induction coils. Since the spot is necessarily of finite width (about 45×10^{-3} in.) and is located in a region of high radial thermal gradient (about 4°F per 10^{-3} in.), inaccuracies in temperature measurement inevitably occur.

Various calibration efforts for this measurement are discussed by Pears and Starrett.[7] They conclude that the micro-optical recorder can be used to measure temperatures up to about 5500°F on the disk outer surface, and could be extended to even higher temperatures. The inherent accuracy of the readings is about ±50° up to 5000°F. However, the recorder slewing speed is approximately the same as the temperature rise in many tests, so that the final outer diameter temperature measurements are inaccurate at high temperatures, and therefore must often be ignored.

Diametral Deformation Measurements

The changes in the disk inner diameter are measured along x and y axes in Fig. 4 by use of a laser tracking device. The laser beams are focused and located with a complex prism system described by Pears and Starrett.[7] Basically, the two orthogonal diameter change measurements are different because the electronic circuitry is slightly different (each corresponding component of the two circuits is different within the manufacturer's tolerances). The output of the x and y measurements is recorded on the same recorder with offset initial points. These initial points are located by use of a tick mark placed on the recorder when the induction coils are turned on. The tick mark is not, however, recorded precisely when the coils are turned on. Pears and Starrett[7] conclude that the maximum diameter change error for a single experiment is 72×10^{-6} in. (the timer error is essentially eliminated by graphically extending the recorder output back to a zero deformation reading).

Summary

The inner diameter temperature measurements are used to determine the approximate temperature distribution in the disk. That is, the theoretical temperature distributions at various times will be shifted in time until the measured time when the predicted inner diameter temperature agrees with the measured inner diameter temperature. The outer diameter temperature is recorded at such a speed that the results are not meaningful. Otherwise, they could be used to further adjust the temperature distributions in the manner discussed for the inner diameter temperature measurements. The diametral deformation measurements are the primary measurements, and are half of the basis for comparison of measured and

Table 2 Coefficients of thermal expansion for ATJ-S(WS) graphite as a function of temperature

Temperature, °F	α_r, 10^{-5}/°F	α_z, 10^{-5}/°F
70	0.1200	0.1720
2000	0.1915	0.2471
3000	0.2194	0.2727
3500	0.2315	0.2864
4000	0.2414	0.2997
4500	0.2547	0.3174

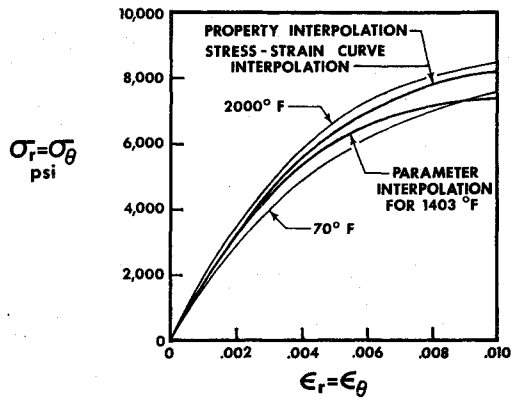

Fig. 5 Temperature interpolation of stress-strain behavior.

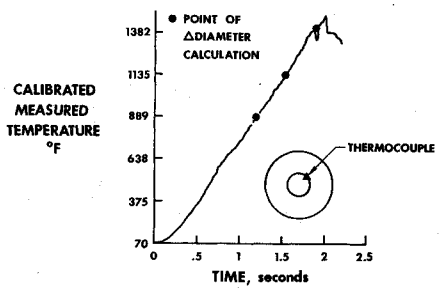

Fig. 6 Disk i.d. temperature vs time.

predicted deformations. The second half, the predicted deformations, is described in the next section.

Prediction of Deformations, Stresses, and Strains

The predicted deformations, stresses, and strains of the wedge-shaped annular disk are obtained with the Jones-Nelson nonlinear material model, which is described in the first subsection. Second, the Jones-Nelson model of ATJ-S graphite is displayed and discussed. Then, the new procedure for temperature interpolation of mechanical properties is described. Next, the predicted inner diameter changes are compared with measured values. Finally, the stresses and strains in the disk are described.

Jones-Nelson Nonlinear Material Model

The Jones-Nelson nonlinear material model is described in Refs. 2-6. Here, we merely reiterate the details essential to our use of the model. Basically, the various secant moduli and Poisson's ratios, all of which are called mechanical properties, in the transversely isotropic stress-strain relations, are approximated with

$$\text{mechanical property}_i = A_i[1 - B_i(U/U_{0_i})^{C_i}] \qquad (1)$$

where A_i are the elastic values of the ith mechanical property, B_i and C_i are related to the initial curvature and initial change

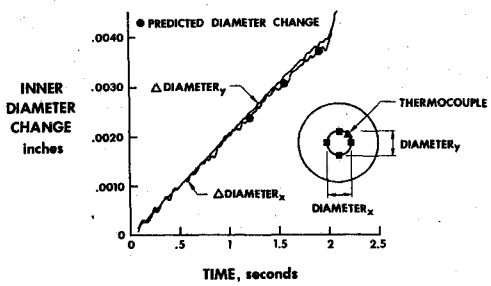

Fig. 7 Disk i.d. change vs time.

of curvature, respectively, of the stress-strain curve[3] (slightly different interpretations exist for Poisson's ratios), and U is the strain energy density of an equivalent elastic system at each stage of nonlinear deformation:

$$U = (\sigma_r\epsilon_r + \sigma_z\epsilon_z + \sigma_\theta\epsilon_\theta + \tau_{rz}\gamma_{rz})/2 \qquad (2)$$

The strain energy density U in Eq. (1) is normalized by U_{0_i}, so that B_i and C_i are dimensionless.

The Jones-Nelson model actually is much more complicated than Eq. (1). For example, in states of mixed tension and compression, the strain energy could be the total strain energy; the tension strain energy U_t for some properties, and the compression strain energy U_c for other properties; or some weighted combination of the tension energy and the compression energy. The strain energy density used in this paper is

$$U_w = (U_t^2 + U_c^2)/U \qquad (3)$$

where U_w is the weighted strain energy. Moreover, all coefficients in Eq. (1) have values that are different in tension than in compression. The final combination of mechanical properties is determined in an iteration procedure wherein the stresses in principal stress directions are a key factor.[5]

Jones-Nelson Model of ATJ-S Graphite

The nonlinear stress-strain behavior of ATJ-S graphite in the plane of isotropy is depicted in Fig. 2. Since the disk is stressed primarily in the r-θ plane, we are concerned mainly with the mechanical properties in that plane. However, many other properties are necessary to perform an analysis. The values of the Jones-Nelson model parameters A_i, B_i, and C_i are given as a function of temperature for all pertinent mechanical properties in Table 1 (the value of U_{0_i} is 1 psi for all properties). Also, the coefficients of thermal expansion are given in Table 2. Both sets of data are obtained from Ref. 1. (The information in Table 1 is not specifically contained in Ref. 1. Instead, the values of A_i, etc., are obtained from stress-strain curve data in Ref. 1 by fitting the Jones-Nelson material model to the data using the JNMDATA computer program,[8] as described subsequently.) The direct moduli E_r and E_z are shown in stress-strain curve form in Ref. 1, along with tables of (constant) Poisson's ratios and coefficients of thermal expansion. The values for E_{rz}^{45} are obtained by observing the relation between the coefficients in Eq. (1) for E_{rz}^{45}, E_r, and E_z measured for ATJ-S graphite at room temperature by Jortner,[9] and applying that relation to the measured data for E_r and E_z at elevated temperatures.

The boxes in Fig. 2 are actual data from Ref. 1, and the curves are Jones-Nelson curves through the data. The curves are obtained by use of the JNMDATA computer program,[8] to which all of the stress-strain curve data are input, along with instructions which describe the points to be used in the calculation of A_i, B_i, and C_i. Obviously, very good fits to the data can be generated with the JNMDATA computer program. Moreover, all stress-strain curves and mechanical property vs strain energy curves can be plotted easily and quickly.

Temperature Interpolation of Mechanical Properties

The data in Tables 1 and 2 are input to a version of the SAAS III finite element stress analysis computer program,[10] which has been modified to use the Jones-Nelson material model. In the use of the new version, called SAAS IIIM, stress-strain data must be generated at temperatures between the values listed in Tables 1 and 2. If the Jones-Nelson parameters A_i, B_i, and C_i for $T=70°F$ and $T=2000°F$ are interpolated for a specific temperature, say 1403°F, which is the inner diameter temperature at $t=1.9$ sec, then the stress-strain curve labeled "PARAMETER INTERPOLATION FOR 1403°F" in Fig. 5 results. However, this stress-strain curve does not lie *between* the two curves from which it is interpolated. On the other hand, if the nonlinear mechanical properties calculated from Eq. (1) for $T=70°F$ and $T=2000°F$ are interpolated (i.e., E_r at 70°F and at 2000°F), then the curve labeled "PROPERTY INTERPOLATION" in Fig. 5 results. Finally, if the points at the same strain energy on the two stress-strain curves are interpolated, then the curve labeled "STRESS-STRAIN CURVE INTERPOLATION" in Fig. 5 results. Obviously, the latter two approaches coincide for all practical purposes. The property interpolation approach is used in SAAS IIIM because it is simpler to program and less expensive to execute than the stress-strain curve interpolation approach.

Inner Diameter Change Predictions

Times late in the test run are selected for correlation of predicted and measured results. Then, the disk should be deforming nonlinearly, i.e., the stresses should be inelastic. The resistivity of graphite changes with temperature, but is not accounted for in prediction of the temperature distributions at various times with the MOATS heat-transfer computer program[11] (in which convection also is not considered). Accordingly, the temperature gradients are lower at all times than predicted. We account for this discrepancy by assuming that a predicted temperature distribution at one time, with specific inner diameter temperature, is the actual temperature distribution at another time when the predicted inner diameter temperature is the same as the measured temperature. The validity of this time-temperature shift hypothesis would be even more plausible if we could also match predicted and measured outer diameter temperatures. However, the outer diameter temperature measurement with a micro-optical recorder is not sufficiently accurate to be relied upon, because the temperature rise is too fast for the recording device speed used for all measurements. Thus, we depend on the inner diameter temperature correlation to determine the times at which the predicted temperature distributions are applicable. These times, $t=1.2$, 1.55, and 1.9 sec, correspond to measured inner diameter temperatures of 889°, 1135°, and 1410°F, whereas the predicted temperatures are 886°, 1130°, and 1402°F, respectively. Revision of these times to force the predicted temperatures to correspond more closely to the measured temperatures is regarded as unnecessary. The actual calibrated inner diameter temperatures are plotted as a function of time in Fig. 6. There, dots are used to denote the times and corresponding temperatures at which the deformations, stresses, and strains are predicted. The predicted deformations should be slightly too low, because the temperature gradient increases with time, and the predicted temperatures are lower than the measured temperatures.

The measured inner diameter changes are shown in Fig. 7 for two orthogonal directions as a function of time. The change of diameter in the two directions is measured with two electronically equivalent circuits. The measurement in the y direction is much less noisy than in the x direction. However, both measurements are sufficiently accurate for the present correlation effort without calibration. The difference in measured deformations in the x and y directions also can be attributed to the fact that the disk hole does not remain perfectly circular. Of course, the hole should remain circular because the material is nominally isotropic in the plane of the hole, and the temperature distribution is axisymmetric about the z axis perpendicular to the plane of the disk. However, the material does not have perfect transverse isotropy, nor is the temperature distribution perfectly axisymmetric.

The predicted inner diameter changes are plotted in Fig. 7 for $t=1.2$, 1.55, and 1.9 sec. These predictions are obtained with the SAAS IIIM finite element computer program for which the disk finite element mesh is shown in Fig. 8. As is obvious from Fig. 7, the predicted deformations are quite close to the measured values. The actual numerical values for the nonlinear deformation prediction are listed in Table 3. There, the elastic deformation predictions, as well as the errors of both predictions relative to the averages of the two perpendicular diameter change measurements, also are given. The nonlinear predictions are consistently from 2.2 to 3.3% below the average measured values (and essentially coincide with the x channel readings). On the other hand, the elastic predictions are 5% lower than the nonlinear predictions at $t=1.2$ sec, 3.6% lower at $t=1.55$ sec, but 3.4% higher at $t=1.9$ sec. Thus, the nonlinear predictions for this body with a strong nonhomogeneous character (because of the temperature gradient and temperature-dependent mechanical properties) are more consistent relative to the measured deformations than are the elastic predictions. However, the percentage differences between the various approaches are not high enough to warrant strong claims of accuracy for the present approach. Basically, the reported agreement between predictions and measurements is a necessary but not sufficient condition for testing the accuracy of the nonlinear model.

In this regard, the principle of elastic strain invariance as discussed by Manson[12] is revealing. He observes that for bodies under thermal loading the strains calculated from an

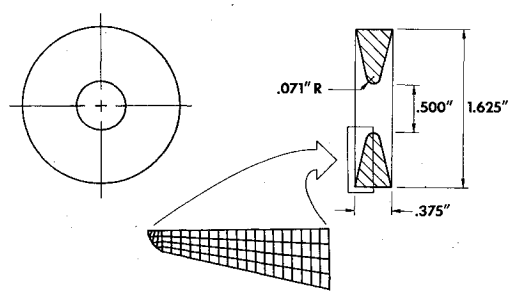

Fig. 8 Wedge-shaped annular disk and finite element idealization.

Table 3 Measured and predicted inner diameter changes

Time, sec	i.d. temperature, °F		Change in internal diam, in.						
	Measured	Used in calculation	Measured			Predicted		% error	
			x channel	y channel	Average	Elastic	Nonlinear	Elastic	Nonlinear
1.2	889	886	0.00230	0.00250	0.00240	0.00220	0.00232	−8.3	−3.3
1.55	1135	1130	0.00300	0.00320	0.00310	0.00292	0.00303	−5.8	−2.2
1.9	1410	1402	0.00365	0.00390	0.00378	0.00380	0.00367	+0.5	−2.9

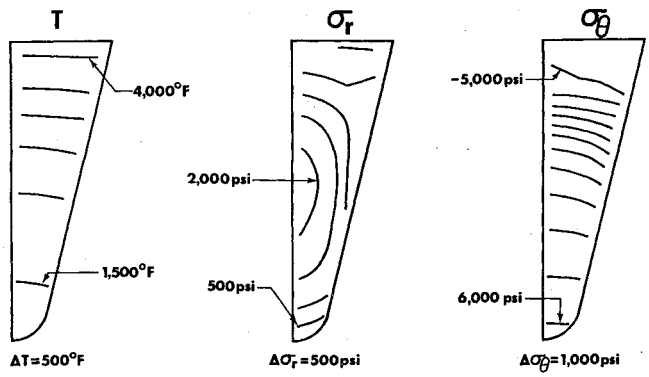

Fig. 9 Temperature and stress distributions at 1.9 sec (contour increments are shown below each plot).

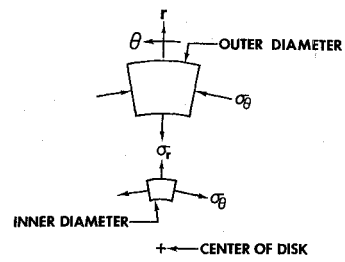

Fig. 10 Free body diagrams of i.d. and o.d. elements.

elastic analysis are remarkably close to the actual strains corresponding to plastic deformation. That is, the actual strains are invariant or essentially independent of the shape of the stress-strain curve (although stresses are admittedly a strong function of the stress-strain curve shape).

In fact, for thermal loading of a singly connected body, the strains are independent of even the elastic moduli if the moduli are constant throughout the body. Under those conditions, the strains are wholly determined from the temperature distribution. Then, for fairly uniform (throughout the body) plastic deformation, the temperature distribution continues to be the primary determining factor for the strain distribution. Hence, the elastic strain predictions are still valid under plastic deformation. On the other hand, if the moduli vary through the body, then the strains are a mild function of the moduli distribution. All of Manson's observations are valid for thermal loading under which yielding is not highly localized, but are not valid when mechanical loading is applied or when unloading occurs.

For the present disk problem, we observe that the annular disk is not a singly connected body, nor are the moduli constant because the temperature varies and the mechanical properties are temperature-dependent. Moreover, the mechanical properties are different in tension than in compression. These three characteristics are violations of the conditions for validity of Manson's principle of elastic strain invariance. Nonetheless, as we will see in the next subsection, the nonlinear strains are quite close to the elastic strains. Thus, apparently, the inhomogeneity of properties is not so severe, nor is the yielding so localized, that the elastic strains are not fairly good approximations of the actual strains. Accordingly, our (strain-related) agreement between predicted and measured inner diameter changes is not conclusive proof that the nonlinear model is valid. However, clearly any thermal loading test also should lead to similarly inconclusive results. We know of no thermal loading test with suitable control over temperature which has more than the necessary, but not sufficient, character of the SoRI thermal stress disk test for validation of nonlinear stress and strain prediction techniques.

Stress and Strain Predictions

The predicted stresses σ_r and σ_θ are shown, along with the corresponding temperature distribution at $t=1.9$ sec, in Fig. 9. Stresses of course cannot be measured; however, their predicted values are examined to determine the degree of stress-strain curve nonlinearity at various times in the thermal stress disk test.

Although we expect σ_θ to predominate, substantial values of σ_r do exist in Fig. 9. These radial stresses always are tensile and can be explained with the aid of the free body diagrams in Fig. 10. There, the view is down the z axis of the disk perpendicular to the plane of the disk. The shear stress τ_{rz} is zero by virtue of axial symmetry of the loading and geometry. The free bodies extend through the (variable) thickness of the disk, so that the shearing stress τ_{rz} is zero. In the body next to the outer diameter, the circumferential stress is compressive. Thus, the radial stress must be tensile to achieve equilibrium, i.e., to balance the component of σ_θ in the negative r direction. At the radial location where the circumferential stress is zero, the radial stress also is zero. Of course, the radial stress is zero on the unloaded inner and outer surfaces. Despite these surfaces of zero radial stress, σ_r can have substantial values elsewhere, because of the small disk inner diameter and the high circumferential stresses to which σ_r is inversely proportional and proportional, respectively. Thus, the disk stress state consists of areas of biaxial tension near the inner diameter, but of mixed tension and compression near the outer diameter. Accordingly, the multimodulus capability of the Jones-Nelson model is essential to accurate stress analysis of the disk.

The stress-strain behavior becomes more and more nonlinear when the test time increases, as we see from the increasing disparity between elastic and nonlinear stresses in Table 4. The disparity increases to nearly a factor of two at $t=1.9$ sec. This disparity is depicted graphically for circumferential stresses and strains in Fig. 11. There, the elastic stresses are too high by nearly a factor of two. However, the elastic strains are not nearly as different from the nonlinear

Table 4 Predicted circumferential stresses and strains

Time, sec	Element	Temperature, °F	σ_θ, psi		ϵ_θ			
			Elastic	Nonlinear	Elastic	Nonlinear	$\Delta\sigma$	$\Delta\epsilon$
1.2	1(i.d.)	887	6,295	4,717	0.00313	0.00336	−25%	+7%
	82(o.d.)	2,890	−5,339	−4,515	−0.00252	−0.00248	−16%	−2%
1.55	1(i.d.)	1,131	8,233	5,671	0.00409	0.00429	−31%	+5%
	82(o.d.)	3,457	− 7,442	−5,501	−0.00308	−0.00307	−26%	0%
1.9	1(i.d.)	1,403	10,608	6,380	0.00527	0.00500	−40%	−5%
	82(o.d.)	4,057	− 9,806	−5,071	−0.00360	−0.00379	−48%	+5%

Table 5 Predicted circumferential stresses and strains at i.d. element 1 and radial displacements at i.d. nodal point 2 at $t = 1.9$ sec

Iteration	σ_θ, psi	ϵ_θ	u_r, in.
1	10,608	0.00527	0.001903
2	5,722	0.00503	0.001841
3	6,543	0.00500	0.001834
4	6,345	0.00500	0.001834
5	6,390	0.00500	0.001833
6	6,380	0.00500	0.001833

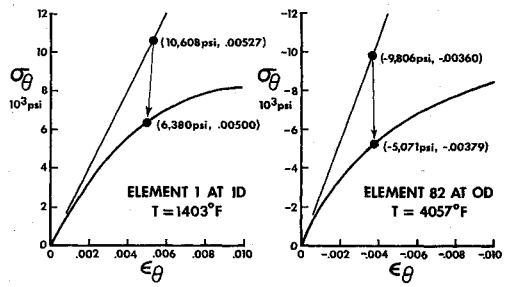

Fig. 11 Degree of nonlinear σ-ϵ behavior; comparison of i.d. and o.d. elastic and nonlinear results.

strains as are the corresponding stresses (in accordance with Manson's principle of elastic strain invariance). Moreover, the elastic strains are not always higher than the nonlinear strains. In fact, the nonlinear inner diameter strain decreases by only 5%, and the nonlinear outer diameter strain *increases* by about 5% from the respective elastic strains. Thus, a failure criterion based on elastic strains is much more accurate than a failure criterion based on elastic stresses. However, even an elastic strain failure criterion is inaccurate because of the 5% error in predicting elastic strains and the fact that the error is sometimes positive and sometimes negative.

The stresses, strains, and displacements converge to the final results in 5, 5, and 6 iterations at $t = 1.2$, 1.55, and 1.9 sec, respectively. Thus, the rapidity of convergence depends on the degree of stress-strain curve nonlinearity, which increases with test time. The inner diameter stresses at $t = 1.9$ sec in Table 5 oscillate with decreasing amplitude about the final results. However, the inner diameter strains and displacements monotonically decrease to the final values.

The energies in each element in the elastic state are well above the energies in the actual nonlinear states. Thus, the energies in the iteration procedure must decrease as the number of iterations increases. Conceivably, the elastic energies could be so much higher than the actual nonlinear energies that the Jones-Nelson model would not converge because of unfavorable numerical characteristics of the various stress-strain curves (first rising, then falling, as for 3000°F in tension in Fig. 2). However, that unfortunate numerical behavior is not found in this problem. If such a difficulty arises, it can be remedied by use of the extended stress-strain curve approaches due to Jones and Morgan.[13]

Concluding Remarks

The Jones-Nelson nonlinear material model is extended from mechanical loading problems for homogeneous bodies to thermal loading problems for nonhomogeneous bodies. The nonhomogeneity results from a temperature gradient over a body with temperature-dependent mechanical properties. Moreover, the model is shown to be valid for materials that have highly nonlinear stress-strain behavior which is different under tension loading than under compression loading. The vehicle for the verification of the model extension is the SoRI thermal stress disk test. The inner diameter changes of this annular wedge-shaped disk made of ATJ-S graphite are predicted with the model to within about 3%. The mechanical properties of ATJ-S graphite are a strong function of temperature level, stress level, and stress sign. However, by a not-strictly-appropriate use of Manson's principle of strain invariance,[12] we can predict the actual strains fairly well with an elastic analysis. Thus, our agreement between nonlinear predictions and measurements is not a conclusive test of the nonlinear model. Nevertheless, because of the agreement (a necessary but not sufficient condition for validity of the model), we consider the present results to be an important step in the qualification of the model for general use in nonlinear material deformation problems.

Acknowledgment

This research was sponsored by the Air Force Materials Laboratory (Contract F33615-75-C-5212) and the Air Force Office of Scientific Research/NA (Grant 73-2532).

References

[1] Starrett, H.S. and Pears, C.D., *Probable and Average Properties of ATJ-S (WS) Graphite,* Southern Research Institute, Air Force Materials Lab. Rept. AFML-TR-73-14, Vol. I, Feb. 1973.

[2] Jones, R.M. and Nelson, D.A.R., Jr., "A New Material Model for the Nonlinear Biaxial Behavior of ATJ-S Graphite," *Journal of Composite Materials,* Jan. 1975, pp. 10-27.

[3] Jones, R.M. and Nelson, D.A.R., Jr., "Further Characteristics of a Nonlinear Material Model for ATJ-S Graphite," *Journal of Composite Materials,* July 1975, pp. 251-265.

[4] Jones, R.M., "Stress-Strain Relations for Materials with Different Moduli in Tension and Compression," *AIAA Journal,* Vol. 15, Jan. 1977, pp. 16-23.

[5] Jones, R.M. and Nelson, D.A.R., Jr., "Material Models for Nonlinear Deformation of Graphite," *AIAA Journal,* Vol. 14, June 1976, pp. 709-717.

[6] Jones, R.M. and Nelson, D.A.R., Jr., "Theoretical-Experimental Correlation of Material Models for Nonlinear Deformation of Graphite," *AIAA Journal,* Vol. 14, Oct. 1976, pp. 1427-1435.

[7] Pears, C.D. and Starrett, H.S., *Polygraphites Subjected to Temperature Stress Loadings,* Southern Research Institute, Air Force Materials Lab. Rept. AFML-TR-73-59, March 1973.

[8] Jones, R.M., *The JNMDATA Computer Program,* Southern Methodist University, April 1977.

[9] Jortner, J., *Uniaxial and Biaxial Stress-Strain Data for ATJ-S Graphite at Room Temperature,* McDonnell-Douglas Astronautics Company, Rept. MDC G3564, June 1972.

[10] Crose, J.G. and Jones, R.M., *SAAS III, Finite Element Stress Analysis of Axisymmetric and Plane Solids with Different Orthotropic, Temperature-Dependent Material Properties in Tension and Compression,* TR-0059 (S6816-53)-1, The Aerospace Corp., June 1971.

[11] MOATS Computer Program, Southern Research Institute undocumented version of OATS in-depth temperature response computer program developed by F.C. Weiler, Weiler Research, Inc., Mountain View, Calif.

[12] Manson, S.S., *Thermal Stress and Low-Cycle Fatigue,* McGraw-Hill, New York, 1966, Chaps. 3 and 5.

[13] Jones, R.M. and Morgan, H.S., "Analysis of Nonlinear Stress-Strain Behavior of Fiber-Reinforced Composite Materials." Presented at the 17th AIAA/ASME/SAE Structures, Structural Dynamics, and Materials Conference, Valley Forge, Pa., May 5-7, 1976; also *AIAA Journal,* to be published.